



## Research Article

# Discrete Element Simulation and Monitoring Analysis of Different Construction Methods of the Shallow Buried Bias Tunnel

Chenyu Ge,<sup>1</sup> Liping Su,<sup>1</sup> Lin Wang,<sup>1</sup> Shuo Xu ,<sup>2</sup> and Pengqiang Yu <sup>2</sup>

<sup>1</sup>Beijing Municipal Road and Bridge Co Ltd, Beijing 100045, China

<sup>2</sup>University of Science and Technology Beijing, Beijing 100083, China

Correspondence should be addressed to Pengqiang Yu; yu\_pengqiang@163.com

Received 30 August 2022; Accepted 30 September 2022; Published 13 October 2022

Academic Editor: Ziyu Tao

Copyright © 2022 Chenyu Ge et al. This is an open access article distributed under the Creative Commons Attribution License, which permits unrestricted use, distribution, and reproduction in any medium, provided the original work is properly cited.

Affected by the bias stress, the mechanical properties of shallow buried bias tunnel construction are complex. The influence of different construction methods on the stability of the portal section of the shallow buried bias tunnel has received significant attention in past studies, but the microscopic mechanism of it has not been properly analyzed. In this study, the discrete element method is used to simulate the construction steps of the three-step method and the single side heading method with and without systematic bolt supports taking Qijiazhuang tunnel as the research object. The tunnel surrounding rock stress, vertical displacement, and surface deformation results under different working conditions are analyzed, and the mechanism of systematic bolt supports is analyzed from microscopic perspective. The results show that the single side heading method can gradually release the load and deformation and better play the supporting capacity of lining; the existence of systematic bolt improves the shear capacity of surrounding rock and enhances the arching effect, thus significantly reducing the vertical displacement of surrounding rock and surface deformation. Finally, compared with the field monitoring data, it is recommended to adopt the single side heading method with systematic bolt support for the construction of the portal section.

## 1. Introduction

With the rapid development of infrastructure construction in China, more and more highway and railway tunnel projects are being built. Due to the numerous mountains and complex geological conditions in China, a large number of tunnels inevitably pass through shallow buried, bias and weak surrounding rock areas [1–5]. The presence of shallow buried bias terrain will induce the bias stress. Meanwhile, the surrounding rock of cave entrance is often broken, affected by soft ground soil and seepage, and the topographic and geological conditions are complicated. Therefore, fully understanding the influence of different excavation methods and supporting schemes on the stability of surrounding rock of the shallow buried bias tunnel has an important reference for guaranteeing the stability of tunnel entrance and surface.

Model experiment and theoretical analysis are important methods to study geotechnical problems [6–10]. Lei et al. [4, 11, 12] studied the fracture mechanism of surrounding

rock of the shallow buried bias tunnel under different bias angles by using model experiment and obtained the variation law of surrounding rock pressure of deep and shallow buried side with bias angle and compared with the calculation method in the standard. Teng et al. [13] derived the calculation formula of surrounding rock pressure of the shallow buried bias tunnel with small spacing considering the construction process and terrain slope by using theoretical analysis and the stress law of surrounding rock under different bias angles, and buried depths were analyzed and compared with the condition that ground surface was horizontal.

With the rapid development of computer and numerical simulation software, the numerical method has gradually become an effective method to analyze geotechnical engineering problems. Since the strong repeatability and the ability to simulate various working conditions, numerical simulation has been favored by many scholars [14–17]. Scholars at home and abroad used numerical methods to

simulate the excavation of the shallow bias tunnel and obtained the stress and deformation law of surrounding rock [1–3, 18]. Some scholars also considered the support and reinforcement conditions of real constructions in the numerical simulation, obtaining the stress and deformation law and evaluating the effect of field construction and reinforcement [5, 19–21]. Dong [19] analyzed the settlement deformation of the tunnel by numerical simulation and evaluated the effect of the existing supporting structure and the effect of the back pressure backfilling reinforcement measures. In addition to evaluating the effectiveness of existing supporting structures, numerical simulation can also be used to optimize construction methods for shallow bias tunnels [22–25]. Zhao et al. [22] simulated the portal section of the shallow buried bias tunnel by using ANSYS software and obtained the construction schemes that meet both the standards and the stability requirements. Numerical simulation can also be used to reveal the stress mechanism of the shallow buried bias tunnel. Yang et al. [26] studied the failure mechanism and treatment measures of the main support of the shallow buried bias tunnel.

The existing simulation is mostly based on the continuum mechanics method, and there are few studies on the mesoscopic mechanism of the stability of the shallow buried bias tunnel. The discrete element method (DEM) is an important method to study the mechanical behavior of discontinuous media from the perspective of mesoscopic force chain [27, 28]. As a typical discontinuous media, it is more appropriate to analyze the stability of surrounding rock of shallow buried bias tunnel excavation from microscopic perspective using the discrete element method (DEM) [29–37]. Therefore, the aim of this study is to use DEM to study the law of surrounding rock stress, displacement, and surface deformation under different support methods during the excavation of the shallow buried bias tunnel and analyze the microscopic mechanism of the shallow buried bias tunnel, taking Qijiazhuang tunnel as engineering background. The development law of cracks in the surrounding rock caused by tunnel excavation, the distribution characteristics of contact force, and the evolution law of pressure arch are analyzed from microscopic perspective. The optimal tunnel excavation method and support measures are obtained by comparing with the field monitoring data.

## 2. Project Overview

The Qijiazhuang tunnel is located in Qijiazhuang village, Mentougou district, Beijing. The starting and ending mileage of the left line is A1K70+075~A1K70+369.14, with the length of 294.14 m, whose maximum buried depth is 29 m. For right line, starting and ending mileage is AK70+076.286~AK70+375, with the length of 298.714 m, whose maximum buried depth is 41 m. The entrance and exit of the tunnel are located in the slope of the foothills. The tunnel portal, mileage A1K70+090~A1K70+195, is shallow buried and bias section, where the angle of surface slope is about 15~35°. The tunnel axis is basically orthogonal to the contour, and the bedrock is exposed above the entrance.

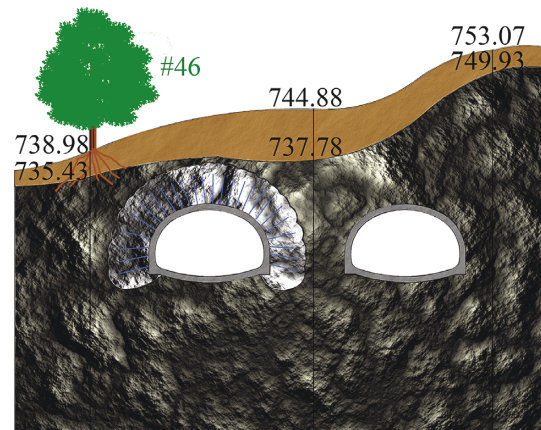


FIGURE 1: Schematic graph of section A1K70+115 of tunnel.

There are more than 60 cypress trees whose diameter is greater than 30 cm on the ground surface of the tunnel. The surface of slope is residual soils with the thickness of 0.5~2.0 m. Beneath the soil are strongly weathered andesites. The bias tunnel and distribution of rock and soil layers are shown in Figure 1, and the longitudinal section of tunnel is shown in Figure 2.

The surrounding rock is highly and moderately weathered, rock mass is broken, and joint fissure develops, and small range of water gushing in surrounding rock of tunnel entrance. According to criteria for surrounding rock mass classification in standard for engineering classification of rock mass (GB50218-2014) [38], the surrounding rock of the Qijiazhuang tunnel is defined as IV-V levels. Figure 3 shows the silts and residual soil on the surface of mountain slope.

Initial lining consists of section steel frame, system bolt and sprayed concrete, and mat reinforcement. Among them, the section steel frame adopts I22b steel with longitudinal spacing of 50 cm; the system bolt adopts  $\phi 25$  bolt, whose length is 4 m, and hollow grouting is adopted. The longitudinal spacing of the bolt is 50 cm, and the circumferential spacing is 100 cm, using the plum-shaped arrangement; the sprayed concrete uses C25 concrete with the thickness of 28 cm.

## 3. Numerical Model

**3.1. Working Conditions.** According to different excavation methods (three-step method and single side heading method) and different support methods (with and without system bolt support), four work conditions are selected and are shown in Table 1.

**3.2. Discrete Element Model Determination.** The numerical model is established according to section A1K+115 of tunnel, and the surrounding rock classification of the section is V level. The buried depth of left and right tunnel is 12 and 19 m, respectively. The width of excavated section of left and right tunnel is 44.71 m, and the height of the section is 11.861 m. Based on elastoplasticity theory, the size of the

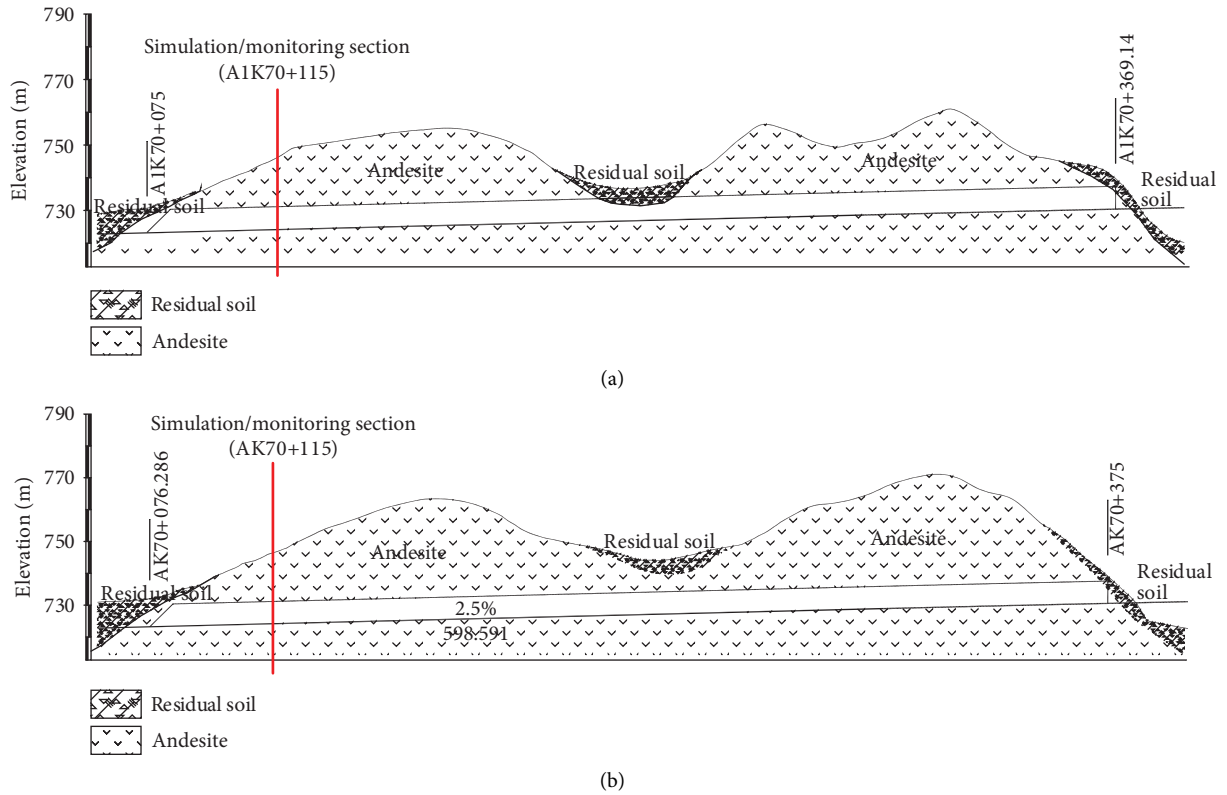


FIGURE 2: Longitudinal profile diagram of the Qijiazhuang tunnel: (a) longitudinal profile diagram of left line; (b) longitudinal profile diagram of right line.



FIGURE 3: Geological features of surface residual soil and surrounding rock.

TABLE 1: Scheme of numerical simulation for different excavations and reinforcements.

Work condition	Excavation method	Support method
1	Three-step method	Initial support (without systematic bolt)
2	Three-step method	Initial support (with systematic bolt)
3	Single side heading method	Initial support (without systematic bolt)
4	Single side heading method	Initial support (with systematic bolt)

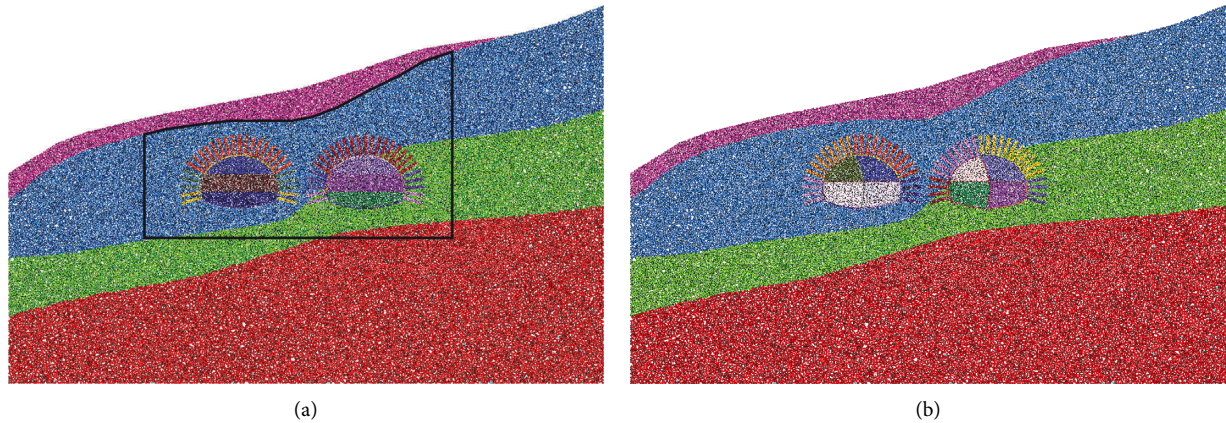


FIGURE 4: Numerical model: (a) three-step method; (b) single side heading method.

model should be 3~5 times as long as the span of the tunnel to reduce the effect of boundary condition. As shown in Figure 4, the width and height of the model are 130 m and 82.67 m, respectively. The tunnel is located at the central axis of the model, the minimum point of the inverted arch is 38.168 m away from the bottom of the model, and the thickness of initial lining is 280 mm. Constraint of horizontal displacement is applied on the left and right boundaries of the model, and constraint of vertical displacement is applied on the bottom of the model, and the top of the model is freedom boundary condition. The system bolt and grout reinforcement range are equivalent to rectangle with 4.5 m length and 0.75 m width.

According to the “Particle-Size Refinement” method, the particles within the specified range are generated. The interparticle contact model adopts the linear parallel bond model, which is suitable for cemented materials such as rock. Besides, in order to improve the calculating efficiency, the radius of particles near the tunnel disperses from 0.035 to 0.255 m, which is shown in domain enclosed by black curve in Figure 4. While the radius of particles in other parts is between 0.255 and 0.367 m, the total amount of particles in the model is 162092. The initial stress of the model is obtained by applying the gravity field with 10.0 gravity acceleration. After equilibrium, the vertical stress at the bottom midpoint is 1.38 MPa, which is close to the stress of 1.264 MPa at the lower boundary obtained by the elastic theory. After excavation, parameters of initial lining are applied.

**3.3. Model Parameters.** Based on the tunnel design instructions, engineering investigation report, and engineering analogy, the macroscopic parameters of geomaterials could be determined. The macroscopic parameters of surrounding rock and strata are shown in Table 2.

According to the data provided by the engineering investigation report, the rock biaxial compression numerical test is adopted. By adjusting and optimizing the microscopic parameters continuously, the model parameters can be obtained by selecting the results of test which are close to the

data of the report. The final micromechanical parameters of each stratum are shown in Table 3. The Mohr–Coulomb strength envelope of the moderately weathered rock is shown in Figure 5. Notably, the simulated cohesion and internal friction angle are in good agreement with the engineering investigation results.

The macroscopic parameters of the initial support are determined based on the equivalent calculation method. The parameters of section steel frame and steel mesh in the initial lining are converted to sprayed concrete, i.e.,  $E_c = E_0 + (A_s \cdot E_s)/A_c$ , where  $E_0$  and  $E_c$  are the elastic moduli of concrete before and after equivalent, respectively,  $E_s$  is the elastic modulus of steel, and  $A_c$  and  $A_s$  are the section areas of concrete and section steel frame, respectively. The systematic bolt is simulated by enhancing the value of parameters of rock mass.

## 4. Simulation Results and Discussion

**4.1. Stress Results.** Figure 6 shows the contact force distributions of the three-step method for each excavation stages (without systematic bolt support) and final stage, and Figure 7 shows the contact force distributions for the final excavation stage of the single side heading method. The horizontal, vertical, and shear stress of the position can be obtained by setting the measure circle. The stress within the circle is calculated by  $\sigma_{ij} = 1/V \sum_c l_i f_j$ , where  $l_i$  is the branch vector, defined as vector connecting center of particles,  $f_i$  is the contact force between particles, and  $V$  is the area of measure circle.

The black and red points in Figures 6(b) and 7 represent the positions of the first three highest horizontal and vertical stress, respectively.

**4.1.1. Three-Step Method.** As shown in Figure 6(a), with the depth enhancing, the contact force distribution of the initial state increases uniformly, and the stress of the deep buried side is greater than that of the shallow buried side [13]. The stress redistribution of surrounding rock is caused by excavation of each section. The decrease of contact force in

TABLE 2: Macromechanical parameters for numerical simulation.

Materials	Modulus of deformation E (GPa)	Poisson's ratio $\mu$	Internal friction angle $\Phi$ (°)	Cohesion c (MPa)	Unit weight $\gamma$ (kN/m <sup>3</sup> )
Residual soil	21e-3	0.35	22	18e-3	18
Highly weathered rock	1.9	0.35	27	0.15	19.0
Moderately weathered rock	1.95	0.35	29	0.25	19.5
Slightly weathered rock	2.1	0.35	29	0.25	19.5
Initial lining	35	0.25	—	—	25
Bolt and grouting	11.0	0.25	30	1.35	20

TABLE 3: Micromechanical parameters for numerical simulation.

Materials	Density $\rho$ (kg/m <sup>3</sup> )	Coefficient of friction $\mu$	Effective modulus $E^*$ (Pa)	Normal-to- shear stiffness ratio $K^*$	Bond effective modulus $\bar{E}^*$ (Pa)	Bond normal-to- shear stiffness ratio $\bar{K}^*$	Tensile strength $\bar{\sigma}_c$ (Pa)	Cohesion $\bar{c}$ (Pa)	Friction angle $\bar{\phi}$ (°)
Residual soil	2000	0.4	50e-6	1	50e-6	1	80e-3	80e-3	32.5
Rock (highly weathered)	2300	0.6	1.0e-8	5.0	1.0e-9	5.0	9.0e-5	3.0e-5	32.50
Rock (moderately weathered)	2350	0.6	2.0e-8	5.0	2.0e-9	5.0	9.0e-5	3.0e-5	32.5
Rock (slightly weathered)	2400	0.6	2.0e-8	5.0	2.0e-9	5.0	9.0e-5	3.0e-5	35
Initial lining	2500	0.8	1.0e-8	5.0	20e-9	10	1.0e-25	1.0e-25	80
Bolt and grouting	2400	0.8	1.0e-8	5.0	6.0e-9	5.0	2.0e-6	8.0e-6	35

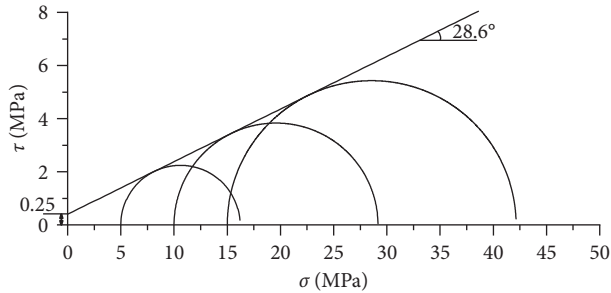


FIGURE 5: Strength envelope under biaxial compression (moderately weathered rock).

lower surrounding rocks is observed due to the release of pressure in excavation section. The rock above the tunnel spontaneously forms the arch structure. The stress in the range of bolt and grouting of work condition 2 are greater due to the adoption of bolt support, as shown in Figure 6(b).

According to the monitoring results of measure circles, the first three highest horizontal stress of work conditions 1 and 2 are 0.479, 0.421, 0.389 MPa and 0.535, 0.527, 0.476 MPa, respectively. Except the point of 0.476 MPa of work condition 2 is located in arch shoulder of right tunnel, other points are all located in arch footing. The first three highest vertical stress of work conditions 1 and 2 are 1.03,

0.984, 0.964 MPa and 1.06, 1.05, 1.01 MPa, respectively. Except these points of 0.984 and 1.06 MPa of work conditions 1 and 2 are located in mid-rock pillar, other points are all located in the lower part of surrounding rock of right tunnel. Obviously, work condition 2 shows the greater stress concentration.

The simulation results show that larger stress concentrations more likely occur at the arch footing, side wall, and mid-rock pillar in three-step method; the system bolt forms a strong bearing structure around the tunnel excavation section, transferring the load of upper rock and soil into depth part, resulting in the stress concentration at the arch footing, mid-rock pillar, and lining. In the actual construction, the support at these positions should be strengthened, and the right-side tunnel should be monitored to ensure the stability of surrounding rock.

**4.1.2. Single Side Heading Method.** As shown in Figure 7, similar with the result of the three-step method, the stress redistributions are caused by the excavation of each drift heading, and the decrease of contact force in lower surrounding rocks is found due to release of pressure of excavated sections. The rock above the tunnel spontaneously forms the arch structure, and the stress in the range of bolt and grouting of work condition 4 are higher. The stress of the deep buried side is greater than that of the shallow buried side due to the influence of terrain bias.

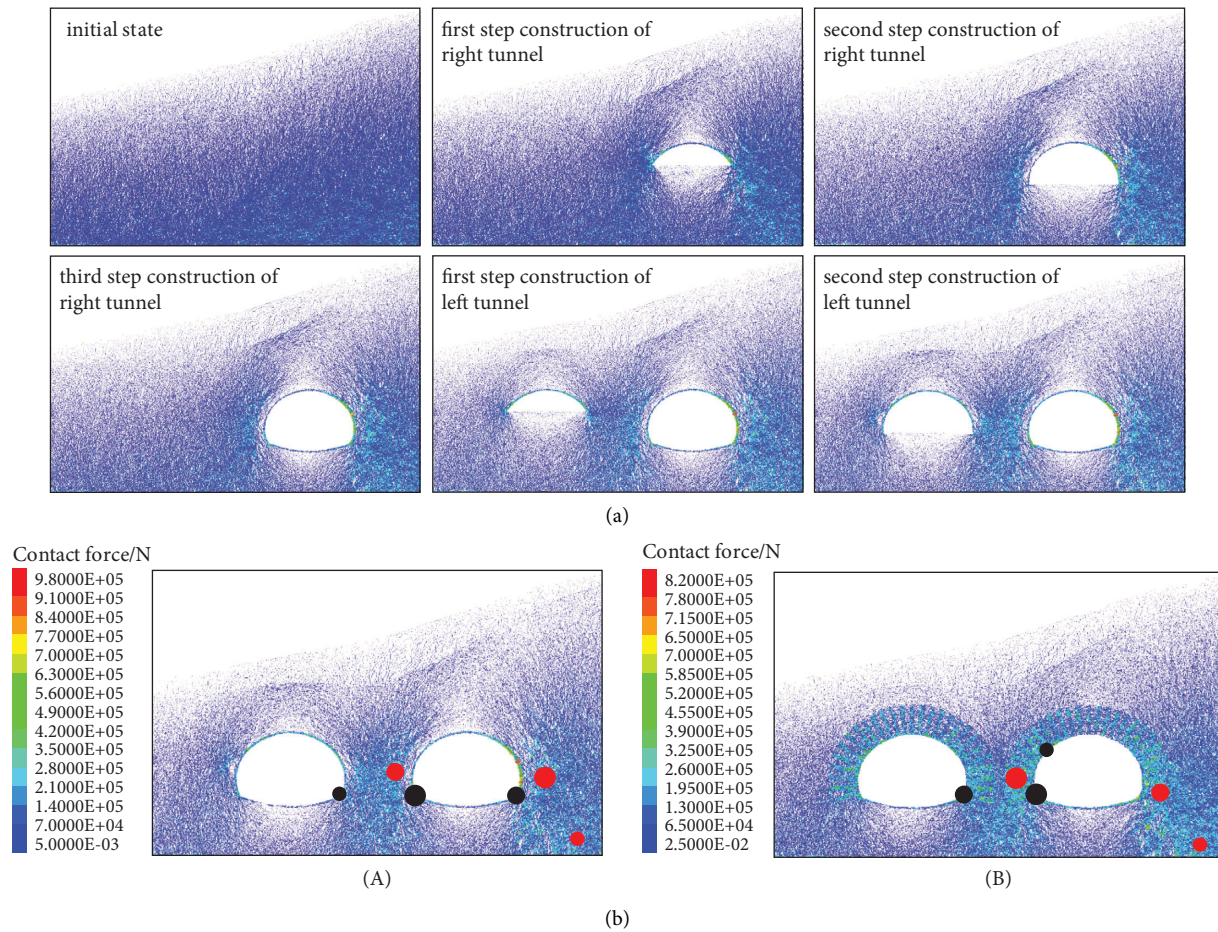


FIGURE 6: Distribution of contact forces of the three-step method: (a) distribution of contact forces for different excavation stages of the three-step method (without systematic bolt support); (b) distribution of contact forces for the final excavation stage of the three-step method: work condition 1 (A), work condition 2 (B).

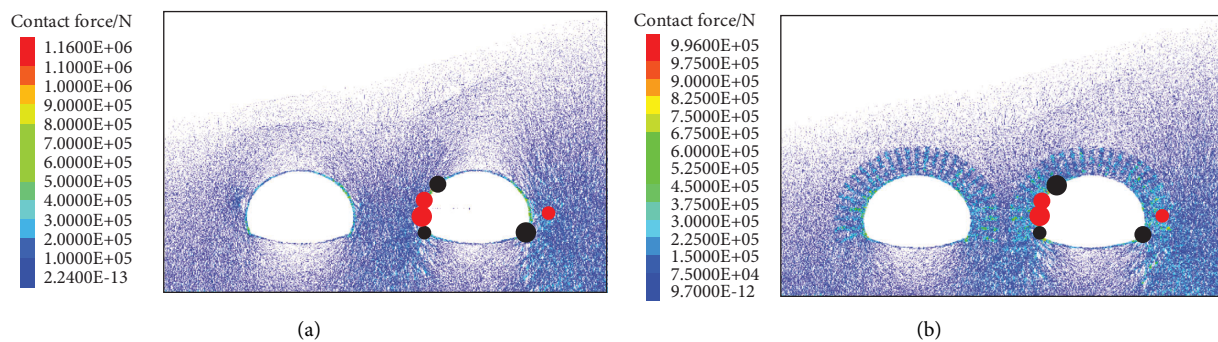


FIGURE 7: Distribution of contact forces for final excavation stage of the single side heading method: (a) work condition 3: the single side heading method without systematic bolt; (b) work condition 4: the single side heading method with systematic bolt.

According to the monitoring results of measure circles, the first three maximal horizontal stress of work conditions 3 and 4 are 0.52, 0.417, 0.41 MPa and 0.603, 0.565, 0.534 MPa, respectively. Except these points of 0.417 and 0.603 MPa located in arch shoulder of right tunnel, all other points located in the arch footing of right tunnel. The first three maximal vertical stress of work conditions 3 and 4 are 1.31,

1.15, 1.05 MPa and 1.19, 1.10, 1.02 MPa, respectively. Except these points of 1.05 and 1.02 MPa located in the right-side surrounding rock of right tunnel, all other points located in the left side wall of right tunnel. It is obvious that arch footing, arch shoulder, and side wall of right tunnel are the points of bearing greater stress, which is a disadvantage to the stability of the tunnel.

In the single side heading method, the positions of maximal stress are lining of right tunnel, which indicates that the single side heading method can give full play of bearing capacity of lining and alleviate surrounding rock stress concentration. Systematic bolt decreased the magnitude of vertical stress, but caused the increase of horizontal stress. Thus, the support at arch footing, arch shoulder, and side wall should be enhanced, and the monitoring frequency of mid-rock pillar should also be enhanced to guarantee stability of surrounding rock.

**4.2. Displacement Results.** Figure 8 shows the layout of surface and surrounding rock displacement measuring points. The displacement contours of different excavation stages of the three-step method and single side heading method without systematic bolt support are presented in Figures 9(a) and 10(a), respectively. Vertical displacement data measured by displacement measure circle are listed in Table 4.

**4.2.1. Three-Step Method.** Figure 9 shows that the vertical displacement of surrounding rock gradually increased with the excavation of tunnel. The position of maximal vertical deformation is the vault of right tunnel, and large heave occurred in the bottom of left and right tunnel. Notably, the vertical displacement is unsymmetrical due to the influence of terrain bias.

For work condition 1, considering the shallow buried depth of left-upper part of right tunnel, the arching effect [39] is limited, which leads to the large vertical displacement of surrounding rock of left-upper part of right tunnel. After excavation of all sections, the vault subsidence of right and left tunnel is stabilized at 22.4 and 14.6 mm, respectively. The maximum vertical displacement occurs in the first step excavation stage of right tunnel, which is 14.5 mm, accounting for 64.7% of the total subsidence. Notably, the three-step method without applying systematic bolt has large vault subsidence, and large proportion of the vault subsidence was caused by the first step excavation.

Due to the use of bolt and grouting support, the bearing capacity of outer surrounding rock of tunnel section in work condition 2 is enhanced. Thus, the magnitude of vertical displacement is primarily depended on the surrounding rock stress, leading larger displacement in deep buried side. After the excavation of all sections, the vault subsidence of right and left tunnel is stabilized at 14.8 and 6.77 mm, respectively. Among them, the maximum subsidence occurred in the first step excavation stage of right tunnel, 11.6 mm, accounting for 78.4% of the total subsidence, followed by the second step excavation stage of right tunnel, 2.9 mm, accounting for 19.6% of the total subsidence. The magnitude of displacement of work condition 2 is less than that of work condition 1 due to the use of systematic bolt support.

**4.2.2. Single Side Heading Method.** Figure 10 shows that the vertical displacement of tunnel is concentrated at the vault,

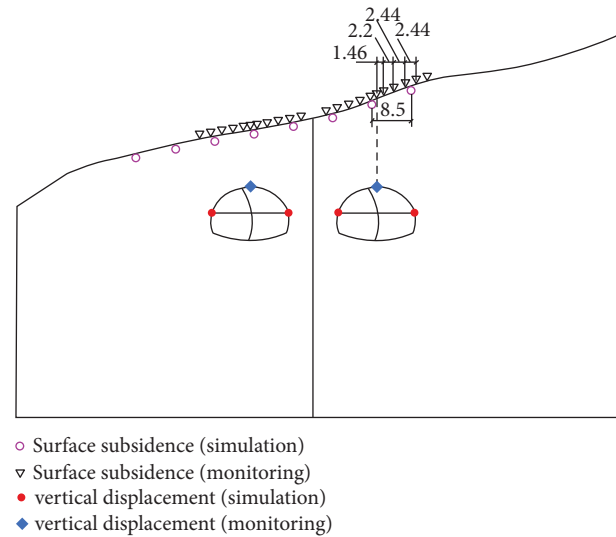


FIGURE 8: Layout of measuring points.

and vertical displacement of deep buried side is larger than that of shallow buried side due to the terrain bias.

Comparing the data in Figures 9 and 10 and Table 4, it can be found that the vault subsidence laws of the three-step method and the single side heading method are significantly different. Taking work conditions 1 and 3, for example, after excavation of left and right tunnels and removal of the temporary supports, the vault subsidence of right and left tunnel of work condition 3 is 14.4 and 10.9 mm, respectively. The maximum vertical displacement occurs in the right-up drift heading construction stage of right tunnel, which is 7.56 mm, accounting for 52.6% of the total subsidence. The vault subsidence and subsidence of arch waist generated by the three-step method is about 1.56 and 2.86 times as large as those of the single side heading method. It can be concluded that the single side heading method can gradually release the load and deformation, which is beneficial to make the support and control the magnitude of deformation.

It can also be noted that the ratio of vault subsidence of right-up drift heading excavation is maximum in all work conditions about the single side heading method. Therefore, the excavation of upper drift heading close to deep buried side is the key procedure that affects stability of the shallow buried bias tunnel, in constructions with the single side heading method. In this sense, for the real construction, the support should be applied in time and the monitoring frequency should be enhanced to prevent large deformation of surrounding rocks and ensure the safety of construction.

The results of vertical displacement in the vault of right tunnel, left arch waist of left tunnel, and arch waist of right tunnel are shown in Figure 11.

According to Table 4 and Figure 11, it can be concluded that the rule of displacement of different work conditions is basically consistent and the magnitude of displacement of the deep buried side is greater than that of the shallow buried side due to the terrain bias. There are sudden changes in the displacement curve of the left tunnel, which is caused by the excavation of the left tunnel, causing the disturbance of the

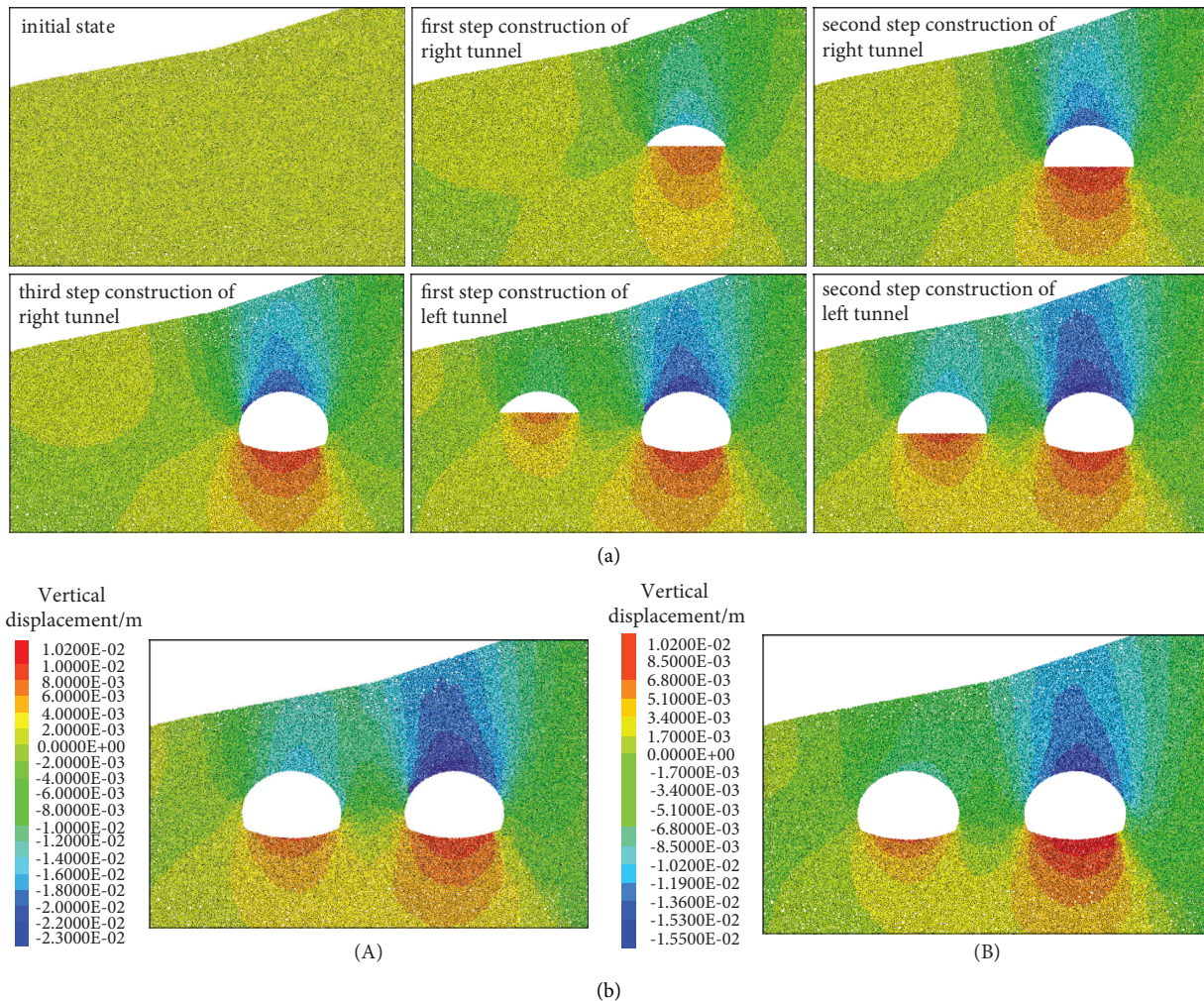


FIGURE 9: Distribution of vertical displacement of the three-step method: (a) displacement contours of different excavation stages of the three-step method (without systematic bolt); (b) distribution of vertical displacement for final excavation stage of the three-step method: work condition 1 (A), work condition 2 (B).

surrounding rock. The subsidence of tunnel vault and arch waist without systematic bolt support is 1.26~1.51 and 0.95~1.53 times greater than cases with systematic bolt. Notably, systematic bolt can reduce vault subsidence of the shallow buried bias tunnel but has deficiency in reducing deformation of side wall, which may even cause the deformation of side wall occurring earlier.

Thus, the entrance section of the tunnel is preferred to use the single side heading method with systematic bolt in real construction to guarantee the stability of surrounding rock and decrease surface settlement. In sections far from the opening, the three-step method with bolt support is suggested to reduce cost and improve efficiency, since the integrity of surrounding rock will be increased and the terrain bias will recede due to the increase of thickness of overlaying soil. It is also noticed that the support at arch footing, arch shoulder, side wall, and mid-rock pillar should be enhanced, and lining should be closed as soon as possible, and the monitoring frequency of mid-rock pillar should be enhanced to guarantee stability of surrounding rock.

**4.2.3. Surface Deformation Results.** Vertical and horizontal displacements of ground surface of different work conditions are shown in Figures 12 and 13, respectively.

It can be observed from Figure 12 that the surface settlement is in the shape of "W." The surface settlement presents evidently unsymmetrical characteristic, which is larger at the deep buried side due to terrain bias and uneven distribution of rock and soil strata. The positions of maximum settlement for all cases are all located above the right tunnel, and some ground heave occurs on the toe of slope. The maximal surface settlement of the three-step method without systematic bolt and the single side heading method without systematic bolt is 17.5 mm and 10.5 mm, respectively. The maximal surface settlement of the three-step method with systematic bolt and the single side heading method with systematic bolt is 11.1 mm and 7.81 mm, respectively. Notably, the single side heading method has a good effect on controlling surface subsidence, and the system bolt support can effectively reduce surface subsidence.



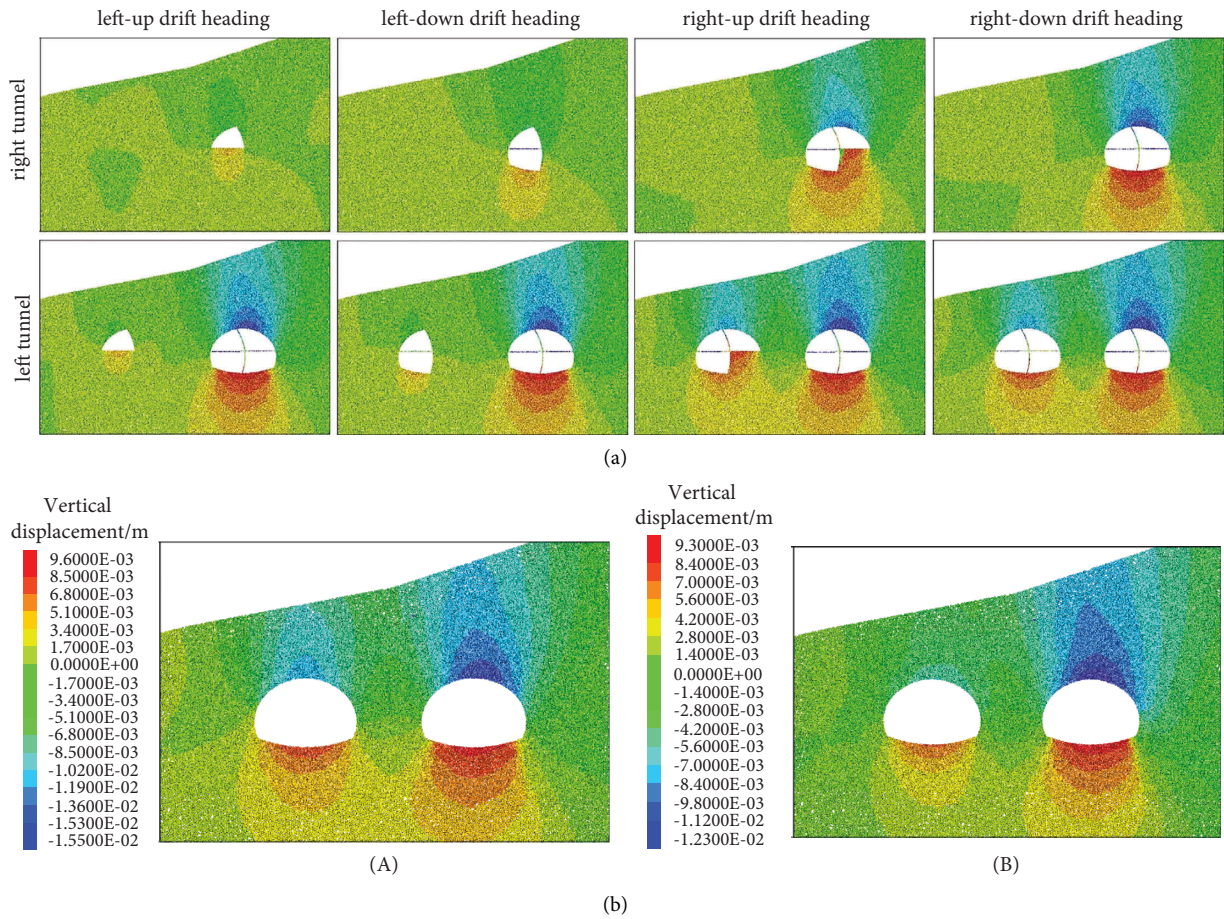


FIGURE 10: Distribution of vertical displacement of the single side heading method: (a) displacement contours of different excavation stages of the single side heading method (without systematic bolt); (b) distribution of vertical displacement for final excavation stage of the single side heading method: work condition 3 (A), work condition 4 (B).

TABLE 4: Micromechanical parameters for numerical simulation.

Work condition	Left tunnel			Right tunnel		
	Vault	Left side wall	Right side wall	Vault	Left side wall	Right side wall
1	14.6	3.12	11.05	22.4	9.69	9.84
2	6.77	2.19	5.02	14.8	7.36	9.69
3	10.9	1.94	5.12	14.4	3.38	6.95
4	4.82	1.27	3.19	11.4	3.55	6.65

In Figure 13, horizontal displacement of ground surface moves right at left side of left tunnel and symmetrical axis between left and right tunnels, while moves left at other sites. The maximal horizontal surface displacement is located in the slope top of right-up side of right tunnel. It can be found that the systematic bolt support decreases the horizontal surface displacement.

### 5. Microscopic Results and Discussion

5.1. Analysis of Fracture of Surrounding Rocks. Figure 14 shows the fracture development of surrounding rocks of the three-step method. According to Figure 14, the number of fractures of work condition 1 is the largest, where the cracks of arch waist of right tunnel extend 12 m upwards and 12 m

downwards. The influence distance of crack to the depth of surrounding rock is about 5.5 m. Systematic bolt support effectively reduces the number of cracks, and the number of fractures in work condition 2 decreased by 28.15% compared with that in work condition 1. Meanwhile, the number of cracks is also influenced by excavation methods. The crack development law of the single side heading method is similar, while the number of cracks is less than the three-step method.

5.2. Analysis of Pressure Arching Effect. Excavation of tunnel broke the equilibrium state of surrounding rock. In order to resist nonuniform deformation, the tangential stress inside the rock mass increases, and the stress path is deflected.

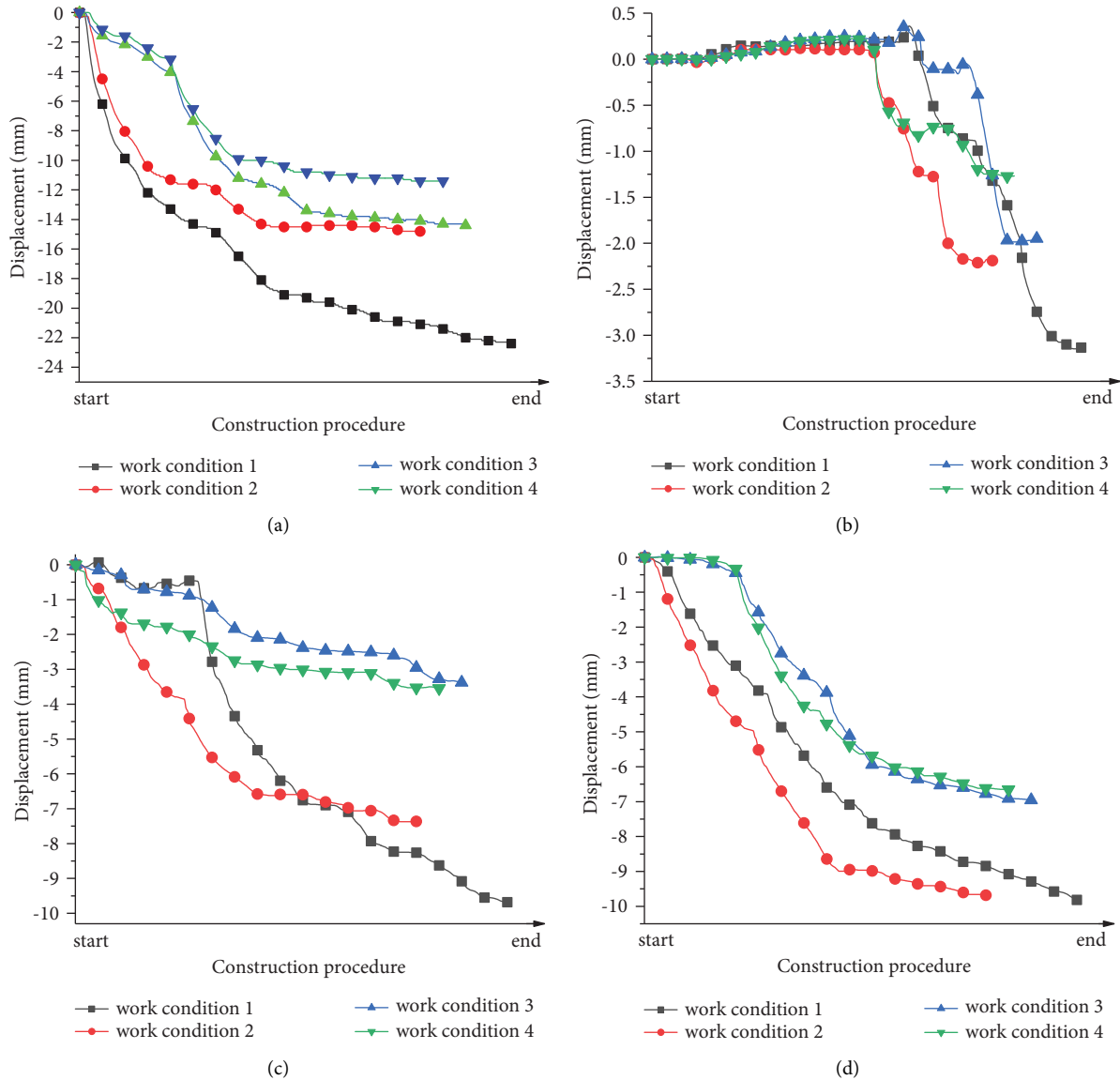


FIGURE 11: Deformation of surrounding rock with different construction methods: (a) vault subsidence of right tunnel; (b) left side wall subsidence of left tunnel; (c) left side wall subsidence of right tunnel; (d) right side wall subsidence of right tunnel.

Thus, a special bearing structure formed, called pressure arch. The development state of pressure arch can be reflected by the arching coefficient  $k$  [40]:

$$k = \frac{\sigma_{\theta} - \sigma_{\theta 0}}{\sigma_{\theta 0}}, \quad (1)$$

where  $\sigma_{\theta}$  and  $\sigma_{\theta 0}$  are the tangential stress of surrounding rock after and before excavation, respectively.  $k < 0$  indicates that the tangential stress is lower than original rock stress and the position is located outside the pressure arch; while  $k > 0$  represents that the position is located in the pressure arch; when  $k = 0$ , the position is the inner boundary and outer boundary of pressure arch.

The layout of measure points of pressure arch is shown in Figure 15. The inner and outer boundaries of pressure arch under different support methods are calculated by linear interpolation of arching coefficient calculated by (1). The

shape of pressure arch after tunnel excavation is shown in Figure 16.

As shown in Figure 16, the inner boundary of the pressure arch is far from the tunnel section in work condition 1, and the inner boundary of the pressure arch coincide with the lining of tunnel, indicating that there are unstable surrounding rocks under the arch. The arching effect is promoted by systematic bolt support; thus, the stability of tunnel is improved.

5.3. *Analysis of Systematic Bolt Mechanism.* Using FISH programming language to count the magnitude of contact force in each direction in the range of bolt and grouting area, the result of microscopic contact force is shown in Figure 17. The position of the line segment in the figure represents the magnitude of the contact force in each direction.

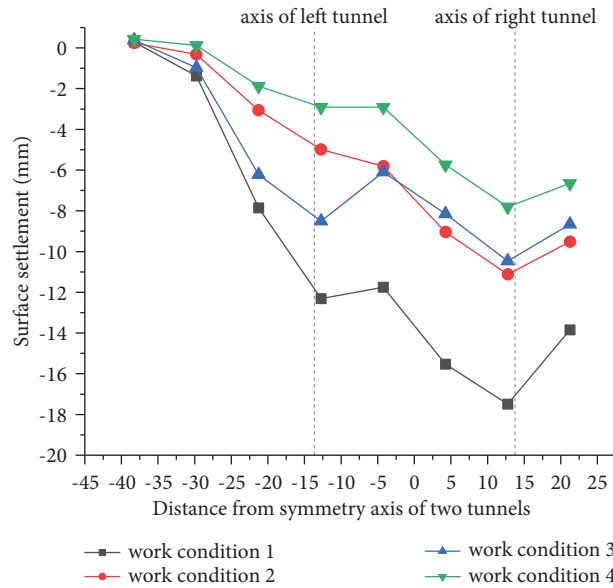


FIGURE 12: Surface settlement with different construction methods.

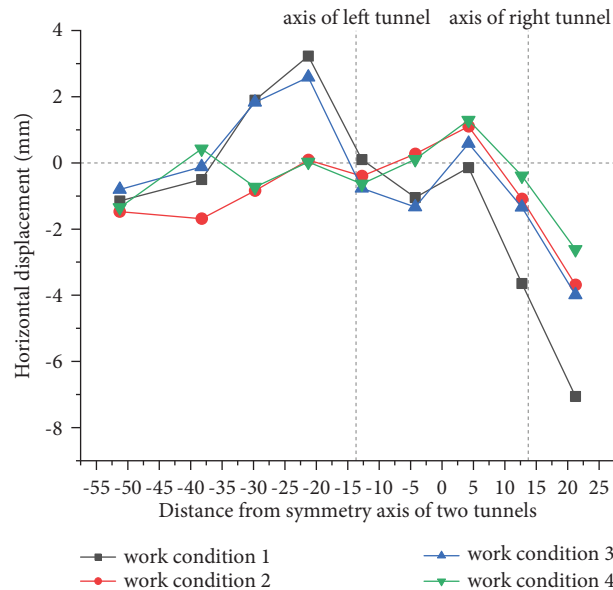


FIGURE 13: Horizontal surface displacement with different construction methods.

As shown in Figure 17, there are some differences in distributions of contact force of surrounding rock at bolt and grout region of different work conditions:

- (1) The contact force in the initial state is in a “peanut-like” distribution. After excavation, the contact force in work conditions without bolt support increased, and its distribution is basically consistent with that of initial state. Under the work condition with bolt support, the contact force increased sharply and the distribution changes obviously.
- (2) Among all work conditions, large contact force occurred in direction 60° and 300°, due to the terrain

bias. In work conditions with bolt support, contact force in direction of 0° and 180° increased, and the distribution of contact force is more rounded, which indicates the surrounding rock stress is more uniform in all directions.

- (3) The reasons why the distribution of contact force changes are as follows: the mechanical parameters of bolt reinforcement region increased by systematic bolt and grouting support and the arching effect is improved by the extrusion reinforcement effect of bolt support (Figure 16(b)). Thus, the contact force distribution changed, leading to variation of stress concentration region.

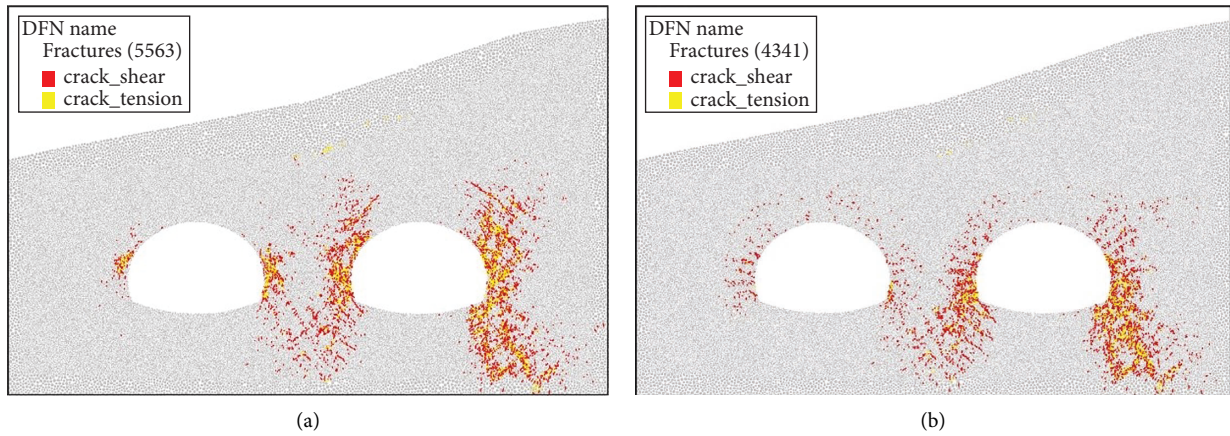


FIGURE 14: Distribution of crack in surrounding rock with different construction methods: (a) work condition 1: the three-step method without systematic bolt; (b) work condition 2: the three-step method with systematic bolt.

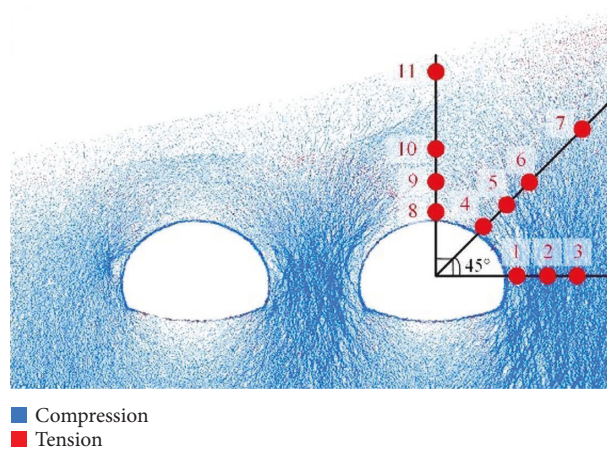


FIGURE 15: Layout of measure point of pressure arch.

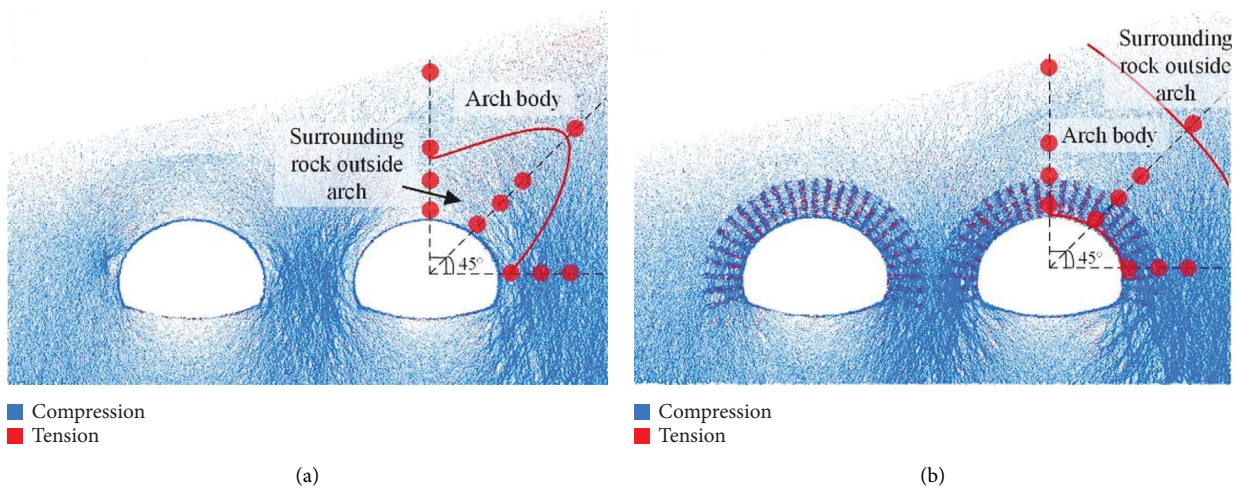


FIGURE 16: Pressure arch distribution diagram: (a) work condition 1: the three-step method without systematic bolt; (b) work condition 2: three-step method with systematic bolt.

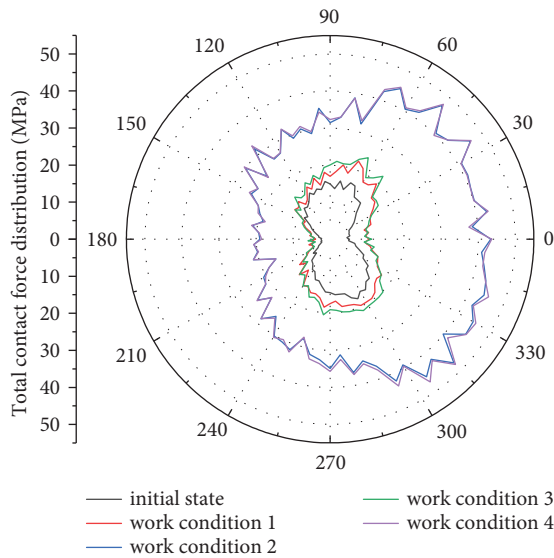


FIGURE 17: Contact force results of bolt reinforcement area.

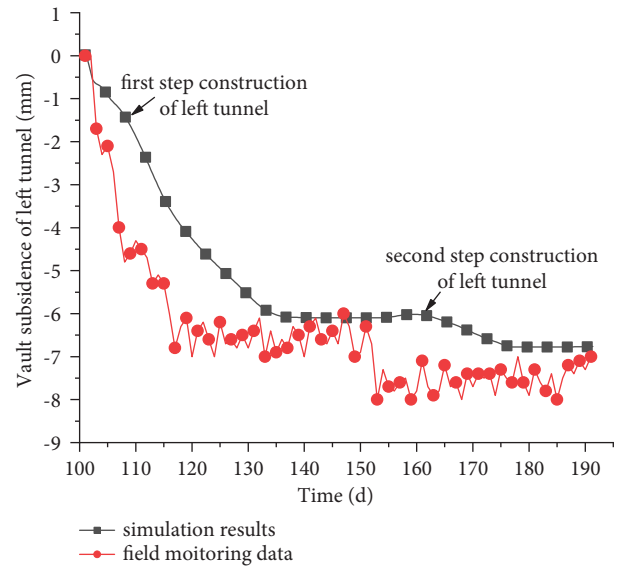


FIGURE 19: Variation curve of accumulated settlement of the vault of left tunnel.

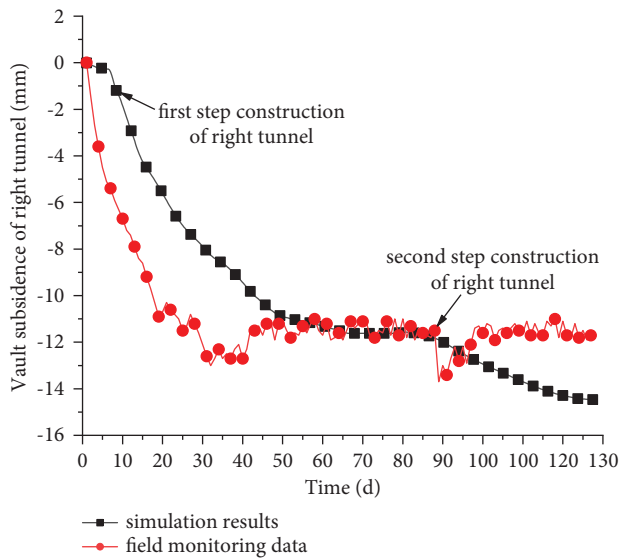


FIGURE 18: Variation curve of accumulated settlement of the vault of right tunnel.

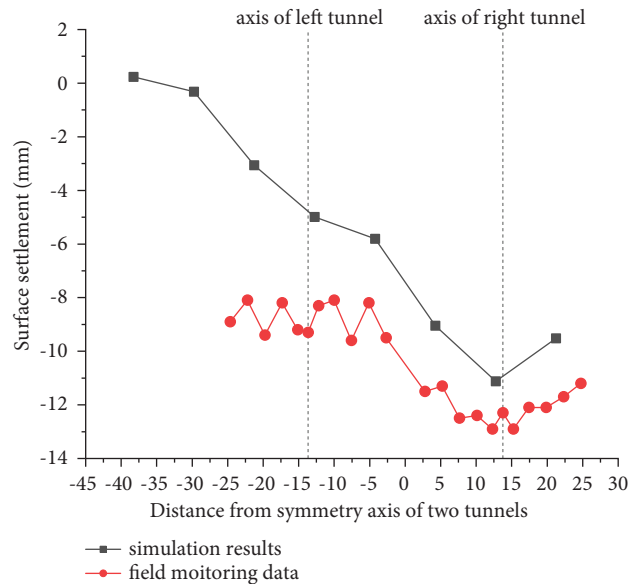


FIGURE 20: Settlement curves of surface.

Therefore, the existence of systematic bolt lead to the formation of active bearing structure at the nearby surrounding rock, which enhanced the bearing capacity of surrounding rocks and improved its ability of sustain upper loading and resist nonuniform deformations.

### 6. Field Monitoring

The displacement of surrounding rock and ground surface are measured during construction of portal part of the tunnel, and the data of displacement of portal part are analyzed [41]. Comparison of measured and simulated vault settlement curves for left and right tunnels is shown in Figures 18 and 19, respectively. Comparison of surface

settlements between field monitoring and simulation results is shown in Figure 20.

As shown in Figures 18 and 19, the vault subsidence curves obtained by numerical simulation and field monitoring are consistent, which grow in “steps” pattern. The vault subsidence of right tunnel increases rapidly at the first step excavation stage and be stable about the 50th day. The vault subsidence fluctuates about the 90th day due to the influence of second step construction. The simulation results matched the monitoring data. The vault subsidence of left tunnel increases rapidly at the first 20 days, and the simulation results agreed with the monitoring data well after the displacement being stable.

Figure 20 shows that the numerical simulation results matched the field monitoring data, and the data of field monitoring are larger.

## 7. Conclusions

Numerical simulations were carried out towards Qijiazhuang tunnel by using the discrete element method. The rule of stress, vertical displacement of surrounding rock, surface displacement, microscopic fractures, and contact force were analyzed in detail. Then, the field monitoring data were compared and analyzed. The following conclusions can be drawn.

- (1) Due to the terrain bias, stress concentration, deformation of surrounding rock, and surface displacement of deep buried side are larger than those of shallow buried side, despite the difference of the excavation method and support method
- (2) The single side heading method can gradually release the load and deformation, which is beneficial to make the support and control the magnitude of deformation. The single side heading method should be adopted as far as possible in the shallow buried bias tunnel.
- (3) The vault subsidence and subsidence of arch waist without systematic bolt are 1.26–1.51 times and 0.95–1.53 times as large as those with systematic bolt. Systematic bolt can reduce the vertical displacement of surrounding rock and the displacement of ground surface greatly. The system bolt support method can be used in the shallow buried bias tunnel to ensure safety in construction. The shape of pressure arch indicates that the existence of systematic bolt increases the shear capacity of surrounding rock; thus, the ability of bearing nonuniform load and deformation of surrounding rock is improved.
- (4) The results of numerical simulation match the data of field monitoring well. The entrance section of the tunnel preferred to use the single side heading method with systematic bolt in real construction. In sections far from the opening, the three-step method with bolt support is suggested because of the relatively lower cost and higher efficiency. Meanwhile, monitoring frequency and support should be enhanced of key positions that influence the stability of the tunnel.

## Data Availability

The data used to support the findings of this study are available from the corresponding author upon request.

## Conflicts of Interest

The authors declare that they have no conflicts of interest.

## Authors' Contributions

Chenyu Ge performed the data analyses and wrote the manuscript; Liping Su contributed significantly to data

analysis and manuscript preparation; Lin Wang established the numerical model and analyzed the results; Shuo Xu reviewed and edited the manuscript; Pengqiang Yu contributed to the conception and methodology of the study. All authors have read and agreed to the published version of the manuscript.

## References

- [1] X. L. Yang and Z. R. Sui, "Numerical simulation of construction sequence for shallow embedded bias tunnels with small clear distance," *Journal of Central South University*, vol. 38, pp. 764–770, 2007.
- [2] X. G. Jin, W. Liu, X. G. Zheng, and H. Ding, "Optimization of excavating sequence for closely spaced bias double-tube tunnels," *Journal of Highway and Transportation Research and Development*, vol. 22, pp. 61–64, 2005.
- [3] X. J. Liu and Y. X. Zhang, "Analysis of reasonable excavation sequence and stress characteristics of portal section of shallow tunnel with unsymmetrical loadings," *Chinese Journal of Rock Mechanics and Engineering*, vol. 30, pp. 3066–3073, 2011.
- [4] M. F. Lei, L. M. Peng, C. H. Shi, W. L. Chuan, and Z. C. Liu, "Model research on failure mechanism and lining stress characteristics of shallow buried tunnel under unsymmetrical pressure," *Journal of Central South University*, vol. 44, pp. 3316–3325, 2013.
- [5] W. X. Gao, W. L. Sun, W. X. Zhou, P. Fu, H. L. Deng, and Y. Y. Zhang, "Numerical simulation and monitoring analysis for construction process of shallow tunnel under unsymmetrical pressure," *Construction Technology*, vol. 40, pp. 48–50, 2011.
- [6] L. H. Xu and M. Ma, "Dynamic response of the multilayered half-space medium due to the spatially periodic harmonic moving load," *Soil Dynamics and Earthquake Engineering*, vol. 157, Article ID 107246, 2022.
- [7] H. Jin, Q. R. Tian, and Z. Li, "Crack development of rebar rust in rubberized concrete using mesoscale model," *Construction and Building Materials*, vol. 321, Article ID 126409, 2022.
- [8] B. X. Yuan, Z. J. Li, W. J. Chen et al., "Influence of groundwater depth on pile-soil mechanical properties and fractal characteristics under cyclic loading," *Fractal and Fractional*, vol. 6, no. 4, p. 198, 2022.
- [9] B. X. Yuan, W. J. Chen, J. Zhao et al., "Addition of alkaline solutions and fibers for the reinforcement of kaolinite-containing granite residual soil," *Applied Clay Science*, vol. 228, pp. 106644–112022.
- [10] B. X. Yuan, M. J. Chen, W. J. Chen, Q. Z. Luo, and H. Z. Li, "Effect of pile-soil relative stiffness on deformation characteristics of the laterally loaded pile," *Advances in Materials Science and Engineering*, vol. 2022, Article ID 4913887, 2022.
- [11] M. F. Lei, L. M. Peng, and C. H. Shi, "Model test to investigate the failure mechanisms and lining stress characteristics of shallow buried tunnels under unsymmetrical loading," *Tunnelling and Underground Space Technology*, vol. 46, pp. 64–75, 2015.
- [12] M. F. Lei, D. Y. Lin, W. C. Yang, C. H. Shi, L. M. Peng, and J. Huang, "Model test to investigate failure mechanism and loading characteristics of shallow-bias tunnels with small clear distance," *J. Cent. South Univ.*, vol. 23, no. 12, pp. 3312–3321, 2016.
- [13] J. Y. Teng, J. X. Tang, C. Zhang, and Y. N. Zhang, "Distribution and control of surrounding rock pressure of shallow buried tunnel under the condition of terrain bias," *Chinese*

- Journal of Underground Space and Engineering*, vol. 14, pp. 761–769, 2018.
- [14] B. Bai, Y. Wang, D. Rao, and F. Bai, “The effective thermal conductivity of unsaturated porous media deduced by pore-scale SPH simulation,” *Frontiers of Earth Science*, vol. 10, Article ID 943853, 2022.
- [15] B. Bai, Q. Nie, Y. Zhang, X. Wang, and W. Hu, “Cotransport of heavy metals and SiO<sub>2</sub> particles at different temperatures by seepage,” *Journal of Hydrology*, vol. 597, pp. 125771–132021.
- [16] B. Bai, R. Zhou, G. Cai, W. Hu, and G. Yang, “Coupled thermo-hydro-mechanical mechanism in view of the soil particle rearrangement of granular thermodynamics,” *Computers and Geotechnics*, vol. 2021, Article ID 104272, 137 pages, 2021.
- [17] X. D. Bai, W. C. Cheng, B. B. Sheil, and G. Li, “Pipejacking clogging detection in soft alluvial deposits using machine learning algorithms,” *Tunnelling and Underground Space Technology*, vol. 113, Article ID 103908, 2021.
- [18] Y. S. Li, K. N. Zhang, X. Yang, and C. B. Huang, “Numerical simulation for the excavation in tunnel construction,” *Applied Mechanics and Materials*, vol. 90–93, pp. 90–93, 2011.
- [19] C. Y. Dong, “Construction deformation control of shallow bias tunnel entrance section,” *Traffic Engineering and Technology for National Defence*, vol. 19, pp. 46–49, 2021.
- [20] L. B. Cai, *Research on the Mechanical Behavior of Unsymmetrical Loading Twin-Arched Tunnels Located on the Shallow Weak Rock Mass*, Tongji University, Shang Hai, 2008.
- [21] H. Jin, J. Su, and C. Zhao, “Relationship between invert-filling disengaging and deformation of shield tunnel using staggered assembled segment,” *KSCSE Journal of Civil Engineering*, vol. 26, no. 4, pp. 1966–1977, 2022.
- [22] Y. G. Zhao, S. J. Shao, and C. L. Han, “Simulation on different excavation construction of the shallow-buried tunnel under the uneven rock pressure,” *Rock and Soil Mechanics*, vol. 30, pp. 509–513, 2009.
- [23] W. Pan, F. Wu, C. He et al., “Construction methods and asymmetric design optimization for shallow-buried tunnels subjected to unsymmetrical loads,” *Tunnel Construction*, vol. 41, pp. 352–361, 2021.
- [24] G. Z. Lu, B. Zhou, F. Xu, G. W. Shang, G. Wang, and S. B. Zhang, “Stability analysis and construction mechanics of shallow buried bias tunnel openings,” *Journal of Shandong University*, vol. 51, pp. 61–70, 2021.
- [25] Y. Liu, J. Hu, and K. J. Wu, “Particle flow code numerical simulation of loess shallow-buried tunnel with different excavation and reinforcement method,” *Journal of Basic Science and Engineering*, vol. 24, pp. 126–138, 2016.
- [26] C. Yang, Z. X. Hu, D. Huang, and F. Guo, “Failure mechanism of primary support for a shallow and asymmetrically loaded tunnel portal and treatment measures,” *Journal of Performance of Constructed Facilities*, vol. 34, no. 1, 2020.
- [27] X. X. Wang, Y. Liu, and P. Q. Yu, “Upscaling critical state considering the distribution of meso-structures in granular materials,” *International Journal for Numerical and Analytical Methods in Geomechanics*, vol. 45, no. 11, pp. 1624–1646, 2021.
- [28] Y. Liu, D. Zhang, S. C. Wu, and P. Q. Yu, “DEM investigation on the evolution of fabric under true triaxial conditions in granular materials,” *International Journal of Geomechanics*, vol. 20, no. 8, 2020.
- [29] T. Wang, “Research on Simulation of Rupture of Rock Mass of Tunnel Based on Particle Flow Method,” in *Proceedings of the The 9th National Conference on Rock Mechanics and Engineering*, Shen Yang, January 2006.
- [30] M. J. Jiang, “New paradigm for modern soil mechanics: geo mechanics from micro to Macro,” *Chinese Journal of Geotechnical Engineering*, vol. 41, pp. 195–254, 2019.
- [31] P. Yuan, S. F. Wang, T. Wang, and Q. Liu, “Construction technology and particle flow code modelling of diversion tunnel support in xigeda stratum,” *Engineering Journal of Wuhan University*, vol. 54, pp. 205–211, 2021.
- [32] R. Xue, “Stability analysis of surrounding rock of tunnel with small clear distance based on discrete element method,” *Fujian Transportation Technology*, pp. 61–65, 2021.
- [33] M. J. Jiang, H. N. Wang, G. S. Li, Y. B. Liao, Y. L. Chen, and C. Q. Wei, “DEM investigation on tunnel excavation of deeply-situated composite rock mass with different strength ratios,” *Chinese Journal of Geotechnical Engineering*, vol. 42, pp. 20–25, 2020.
- [34] M. J. Jiang, H. X. Pang, H. N. Wang, Y. L. Chen, and Y. B. Liao, “Discrete element analysis on excavation failure mechanism of deep-buried tunnel in composite rock mass,” *Chinese Journal of Underground Space and Engineering*, vol. 16, pp. 702–709, 2020.
- [35] B. Bai, S. Jiang, L. Liu, X. Li, and H. Wu, “The transport of silica powders and lead ions under unsteady flow and variable injection concentrations,” *Powder Technology*, vol. 387, pp. 22–30, 2021.
- [36] B. Bai, T. Xu, Q. Nie, and P. Li, “Temperature-driven migration of heavy metal Pb<sup>2+</sup> along with moisture movement in unsaturated soils,” *International Journal of Heat and Mass Transfer*, vol. 153, 2020.
- [37] B. Bai, G. c. Yang, T. Li, and G. s. Yang, “A thermodynamic constitutive model with temperature effect based on particle rearrangement for geomaterials,” *Mechanics of Materials*, vol. 139, Article ID 103180, 2019.
- [38] *Ministry of housing and urban rural development of the people’s Republic of ChinaGBT50218-2014 Standard for Engineering Classification of Rock Mass*, China Planning Press, Beijing, 2014.
- [39] X. D. Liang, J. Zhao, and H. W. Song, “Experimental and numerical analysis on the arching action from stress adjusting in surrounding rocks,” *Journal of Engineering Geology*, vol. 20, pp. 96–102, 2012.
- [40] H. W. Song and X. L. Du, *Pressure Arch in Vicinity of Geotechnical Opening and its Characteristics*, Coal Industry Press, Beijing, 2012.
- [41] Q. W. Xu, P. P. Cheng, P. S. Su, J. T. Dong, and G. Z. Chen, “Study on construction mechanical properties of the shallow tunnel entrance under unsymmetrical pressure,” *Chinese Journal of Underground Space and Engineering*, vol. 13, pp. 1311–1318, 2017.